Electronic Supplementary Material (ESI) for Chemical Science.
This journal is © The Royal Society of Chemistry 2022

Supplementary information for:

Electrochemically Driven C-N Bond Formation from CO_2 and Ammonia at the Triple-Phase Boundary

Junnan Li[a] and Nikolay Kornienko[a]*

[a]*Department of Chemistry, Université de Montréal, 1375 Ave. Thérèse-Lavoie-Roux, Montréal, QC H2V 0B3*

*email: Nikolay.kornienko@umontreal.ca

Characterization:

Scanning electron microscopic (SEM) images and EDS were measured using a JEOL JSM-7600F Field Emission SEM microscope. Transmission electron microscopic (TEM) images were performed on JEOL JEM-2100F FEG-TEM, operated at 200 kV.

Electrochemistry and product quantification:

Linearly sweep voltammetry (LSV) was accomplished using a Bio-Logic SP-200 Potentiostat (BioLogic Science Instruments, France). A three-electrode system has been employed by applying the carbon cloth gas diffusion layer (GDL-CT (W1S1009, Fuel Cells Etc.) as the working electrode, Ag/AgCl as the reference electrode and a glassy carbon rod as the counter electrode. While a Hg/HgOH reference is preferred for alkaline conditions due to its higher stability, we needed a small Ag/AgCl electrode to fit within our cell and referenced it periodically to a master Ag/AgCl electrode to ensure that there was no significant potential drift.

The preparation of working electrode followed steps: 10 mg Cu (Alfa Aesar, Copper Nanopowder, 99.9% APS 20-50 nm, Lot P11F044) or CuO (Alfa Aesar, Copper(II) Oxide, nanopowder, Lot Y19E022) commercial catalyst powder (20-50 nm particle size) was added into a mixture with 100 μL H_2O, 300 μL ethanol, 25 μL Nafion (5% wt.). After ultrasonic mixing for 10 minutes, 100 μL of the catalyst ink was dropped onto the carbon cloth and allowed to dry naturally under ambient conditions. This led to a Cu loading of approximately 2 mg/cm^2. 1M KOH solution with different amounts of NH_4OH was used as the electrolyte in all of the measurements. The LSVs were measured in the range of 0.7 ~ -0.98 V (vs. RHE) at a sweep rate of 20 mV s^{-1}. Potentiostatic electrolysis was conducted in a gas diffusion electrode (GDE) cell. Before each electrolysis experiment, 1 mL electrolyte was added into the cell, the flow rate of CO_2 is 6mL/min. All reactions were carried out at room temperature (23 ± 1 °C). Bulk electrolysis was carried out with

0.3 M NH_3 for Cu and 1.6 M NH_3 for CuO as these were the experimentally optimized conditions for C-N product generation rates. Because of the high gas generation rates and bubbling, we opted to carry out measurements in static mode (no flow) and in a 1-compartment cell. While this likely led to some crossover, product re-oxidation at the counter electrode, and an underestimation of the reaction efficiency, this geometry was nonetheless more optimal to minimize electrolyte volume and overcome the bubbling issue.

NH_3 was only fed through the liquid phase (as NH_4OH) while CO_2 was only added in through the gas phase. Further, no products were detected in the gas phase via GC analysis beyond CO, CH_4 and H_2.

In order to quantify the products of the reaction, gas chromatography (GC, SRI 8610C) and NMR (Bruker AVANCE II 400 se) were performed to reveal the content and composition of the gas and liquid products respectively. A sealed GDE cell was used and connected with the GC. The CO_2 flow rate employed was 6 mL/min and the products were probed in flow mode as the outlet from the GDE cell flowed directly through the GC. For NMR analysis, 400 μL liquid electrolyte after an electrolysis run was mixed with 400 μL D_2O to quantify liquid products. For NMR measurements, products were quantified using DMSO as an internal standard and calibration curves for several main products in the liquid phase like formate, acetate and ethanol (Fig. S1). Gaseous products were similarly quantified through the integration of peak area corresponding to various products, which were first measured with a series of calibration curves (H_2, CO, CH_4, C_2H_6…). The GC measurements were also collected in flow mode at 6 SCCM CO_2 flow with N_2 as the carrier gas in the GC. There was no evidence of nitrogenated products in the gas phase from GC measurements.

Typically, liquid products were acquired after 30 minutes of electrolysis. The Faradaic efficiency (FE) was calculated by using the following formula:

$$\varepsilon_{FE} = \frac{\alpha n F}{Q}$$

where α is electron transfer numbers, n is the moles of the products, F is the Faraday constant (96485 C mol^{-1}), Q is the charge passed in total during the reaction.

In-situ infrared (IR) spectroscopy:

IR spectra were acquired on a ThermoFischer Nicolet 380 FTIR-ATR with a ZnSe ATR crystal that was coated with a diamond surface. Typically, 200 scans were acquired for each measurement. A three-electrode GDE cell was used for the in-situ IR experiment. Cu wire was used as counter electrode, Ag/AgCl was used as reference, the above carbon cloth with CuO or Cu as working electrode. The electrolyte employed was 1M KOH with or without NH_4OH under a constant CO_2 gas flow. Thecatalyst, deposited onto a carbon cloth gas diffusion layer (coated with a microporous layer) was facing downwards towards the ATR crystal, with a thin electrolyte layer between. The working electrode was gently pressed with a porous foam stud so that there was still ample gas permeation into the triple-phase boundary that was being probed with the IR evanescent wave.

Raman Spectroscopy: Raman Spectra were collected using a Renishaw Invia system with a 785 nm laser having a 5mW output power. The laser line focus illumination technique was used that spread the laser intensity out over a line and minimized the power concentrated at any one spot. The spectra were collected at full intensity power and a typical collection time was 60 seconds. A water immersion objective (numerical aperture of 0.7, working distance of 1mm) was used to maximize signal intensity. Raman measurements were performed in a standard 3-electrode configuration instead of adapting to a gas-diffusion electrode as an initial test. For *operando* Raman measurements, Ag/AgCl reference and carbon cloth were used as reference and counter electrodes. N_2 or CO_2 purged 1M KOH or 1M KOH + NH_4OH were used as the electrolyte solutions. The working electrode consisted of Cu NPs loaded onto a Toray carbon paper electrode at approximately the same degree of catalyst loading as for the GDE. For surface-enhanced Raman measurements, a silver foil was roughened in a 0.1M KCl solution by cycling the potential between -0.2 to 0.4V vs. Ag/AgCl at 10 mV/s for 4 cycles. The roughened foil was rinsed and dried under ambient conditions prior to use. A drop of approx. 50 µl of the electrolysis solution was added overtop and measured with an immersion objective and 514 nm laser, operating at approx. 1 mW output power for 60 seconds.

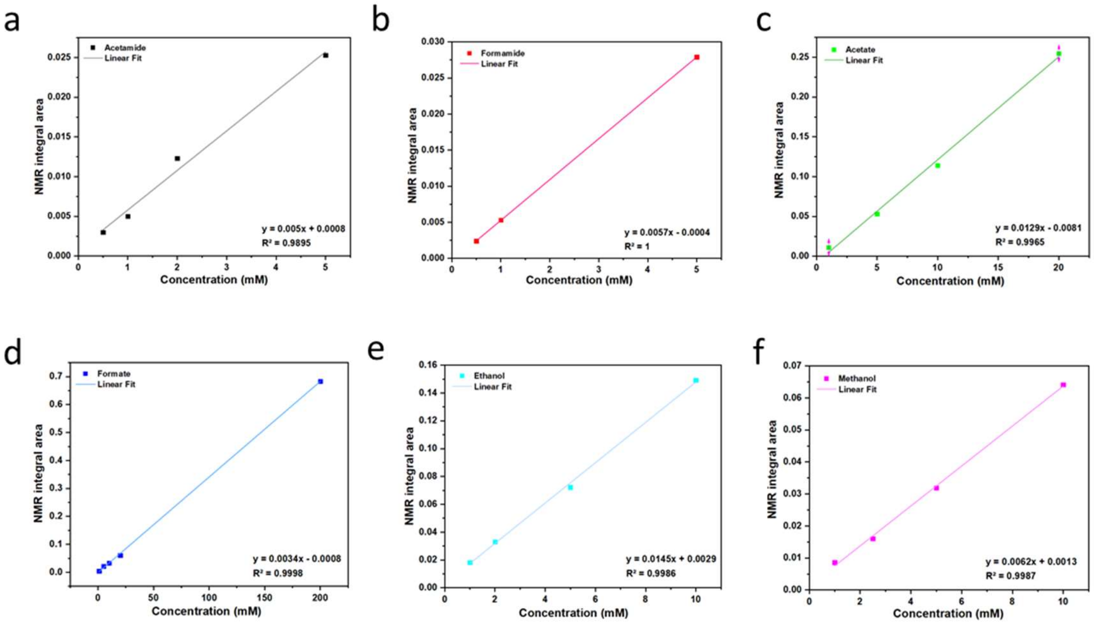

Figure S1: NMR calibration curve of (a) Acetamide; (b) Formamide; (c) Acetate; (d) Formate; (e) Ethanol; (f) Methanol. The relative peak area is plotted vs. that of the DMSO internal standard.

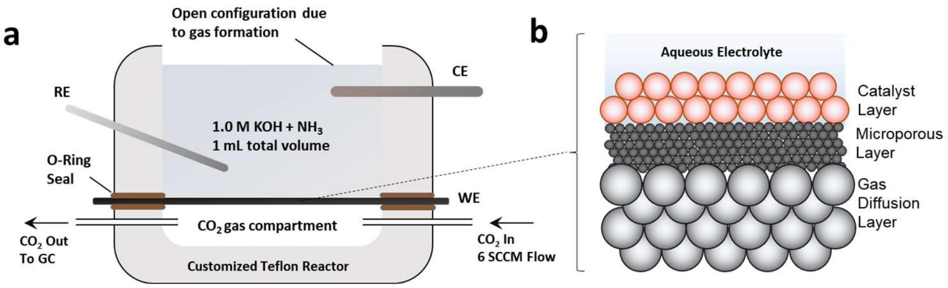

Figure S2: Simplified schematic of CO_2 reduction reaction cell that enabled high-sensitivity detection of liquid products through the use of minimal (1mL) total electrolyte volume (a) sitting overtop of a gas-diffusion electrode (b). An open configuration was employed as gas bubbles generated throughout the reaction process prohibited using a conventional configuration.

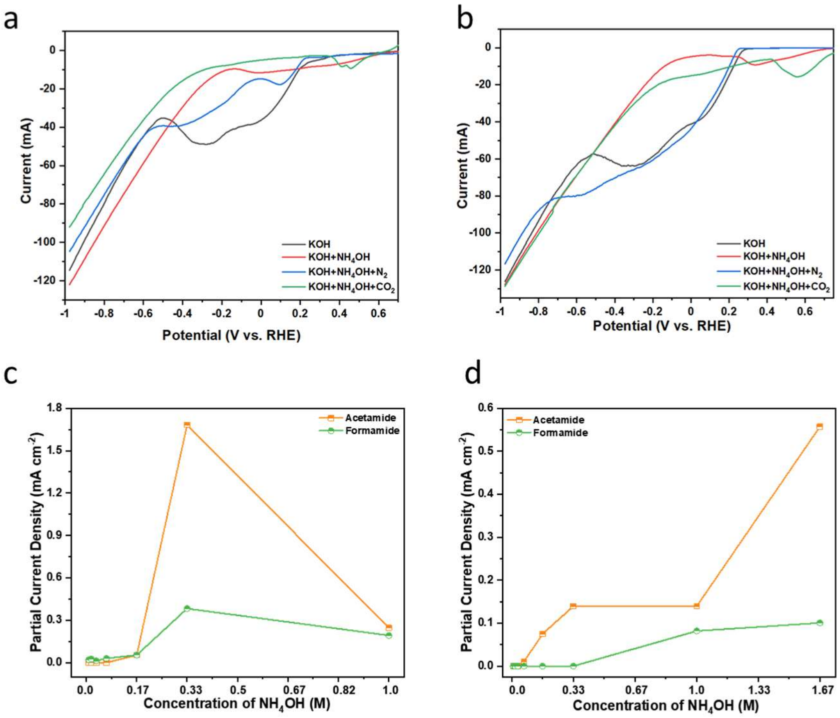

Figure S3. LSV curves under different gas environment of (a) Cu; (b) CuO catalyst in different electrolytes. Partial current densities for C-N products from an initial screening of selecting optimal NH4OH concentrations to add to the electrolyte were also different for Cu (c) and CuO (d).

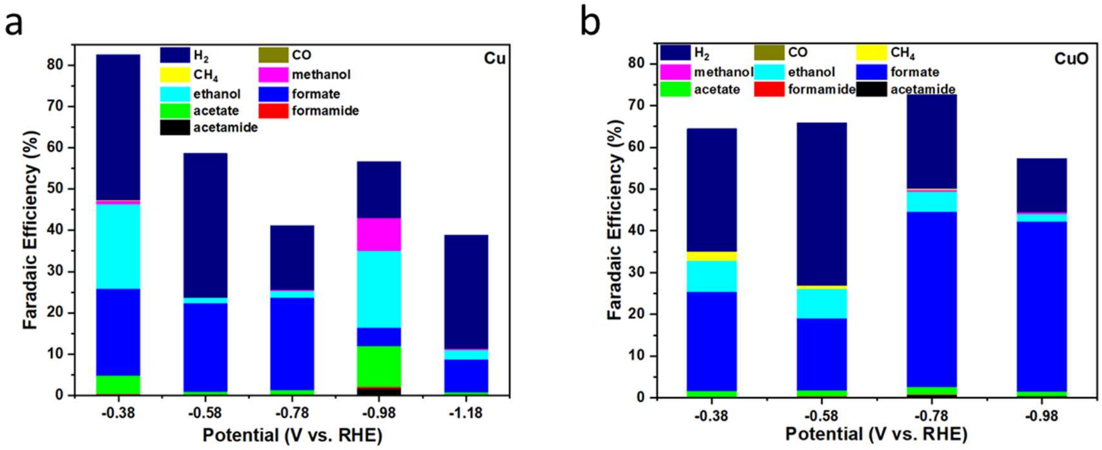

Figure S4: Total product quantification for Cu (a) and CuO (b) catalysts.

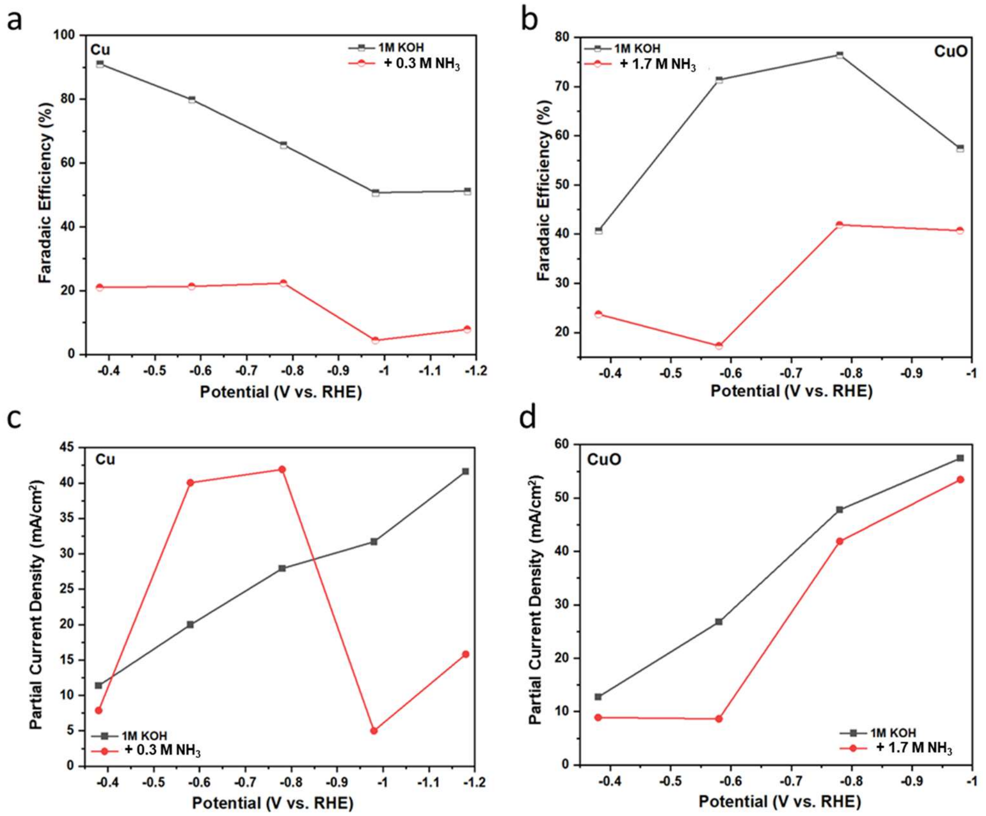

Figure S5: Faradaic efficiency and partial current density for formate production in the absence and presence of NH_3 for Cu (a, c) and CuO (b, d) catalysts.

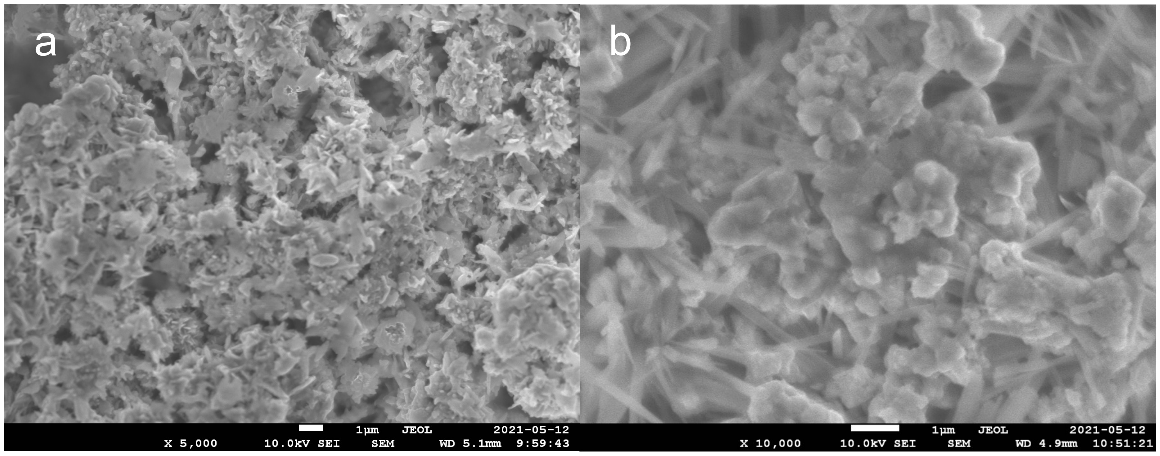

Figure S6: SEM images of (a) CuO and (b) Cu after a typical controlled potential electrolysis reaction.

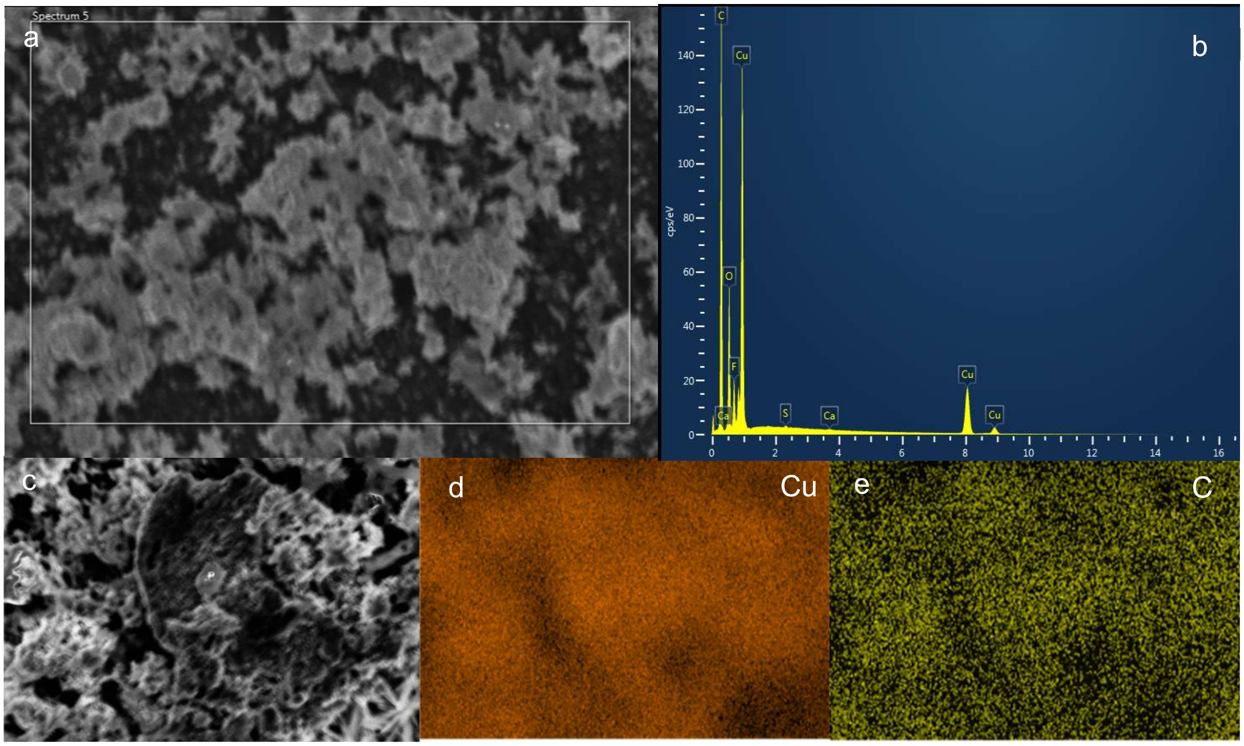

Figure S7. (a, c) SEM images of the EDS area; EDS of CuO/C catalyst before reaction (b) EDS spectra; (d) Cu and (e) C element mapping after the reaction (30 min at -0.98V vs. RHE)**.**

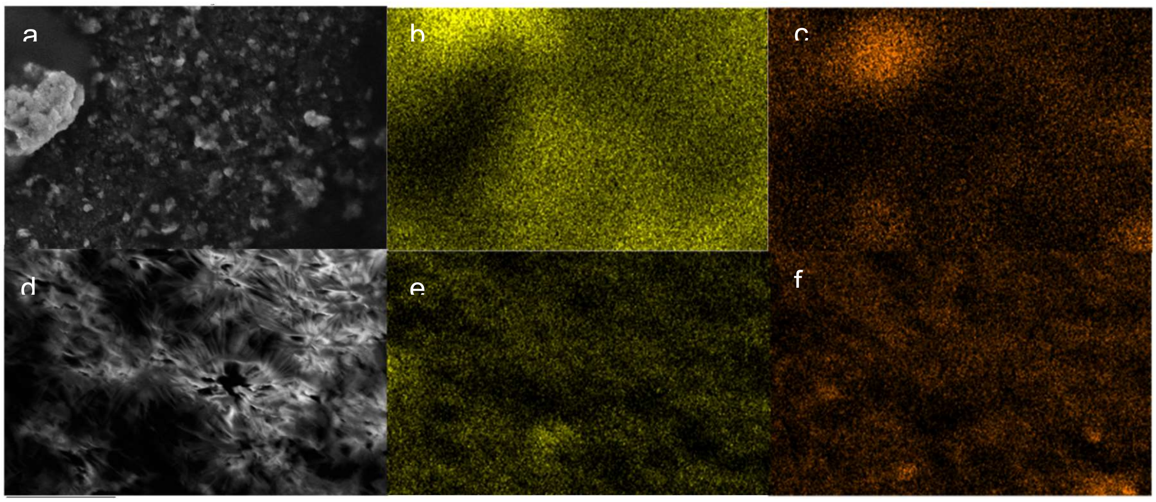

Figure S8: SEM image (a) and elemental mapping of Cu (b) and C (c) before electrolysis. After electrolysis (30 min at -0.98V vs. RHE) an equivalent SEM image (d) and Cu (e) and C (f) elemental mapping was acquired for Cu catalysts.

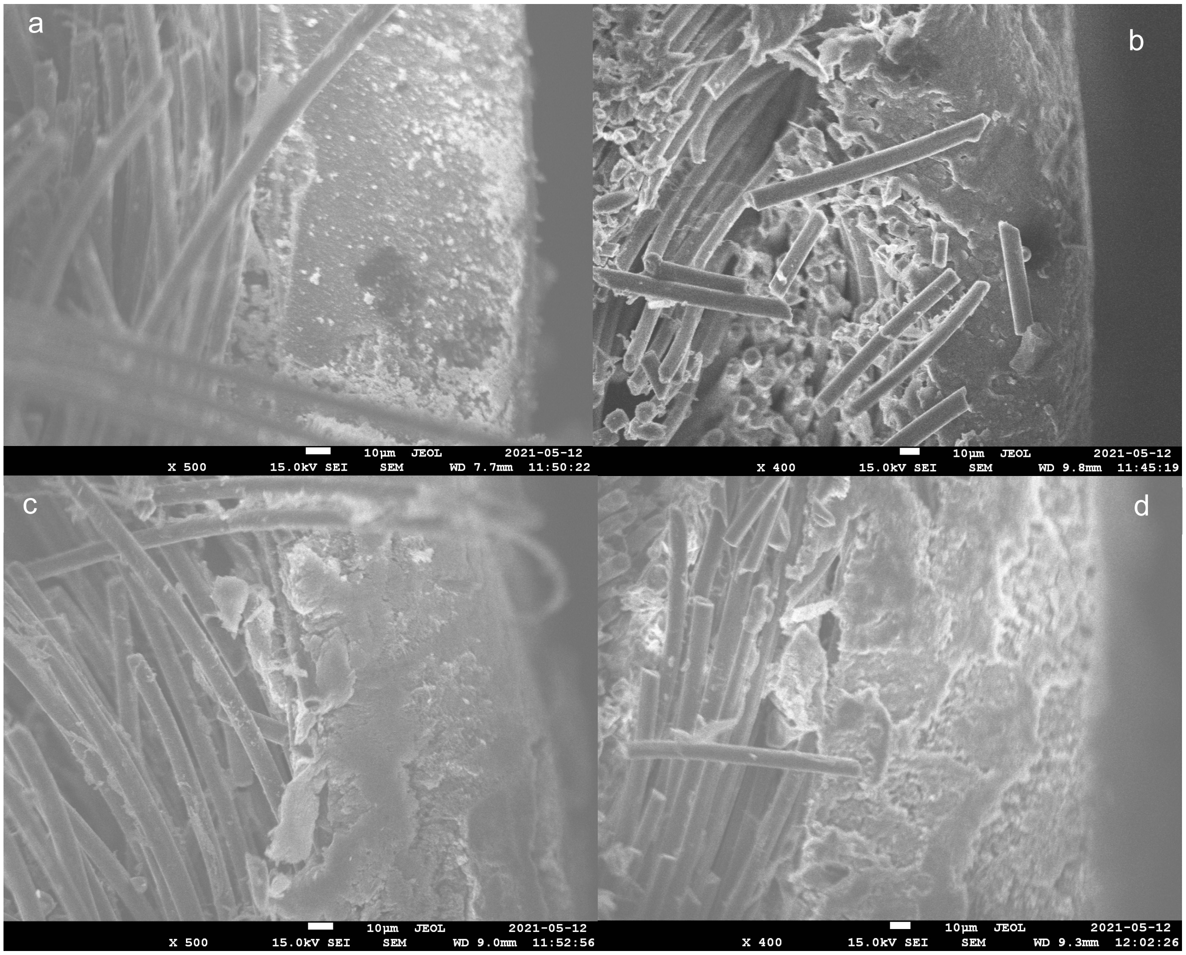

Figure S9: SEM images of the cross session (a) CuO/C before reaction; (b) CuO/C after reaction; (c) Cu/C before reaction; (d) Cu/C after reaction.

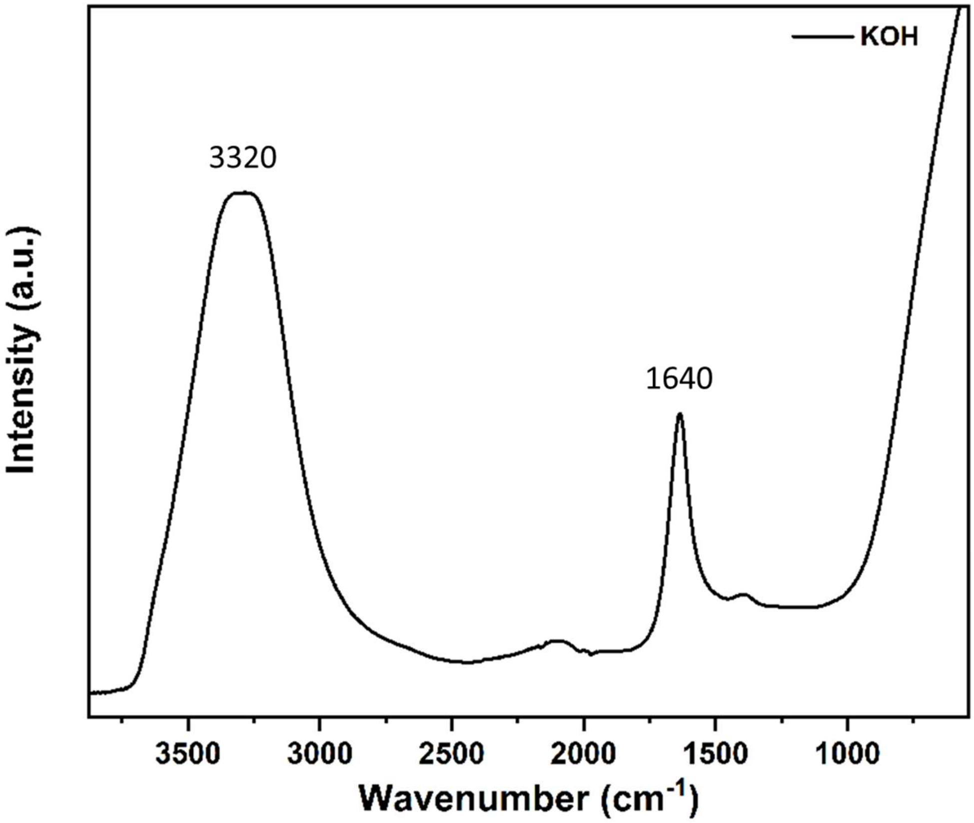

Figure S10: IR spectrum of 1M KOH

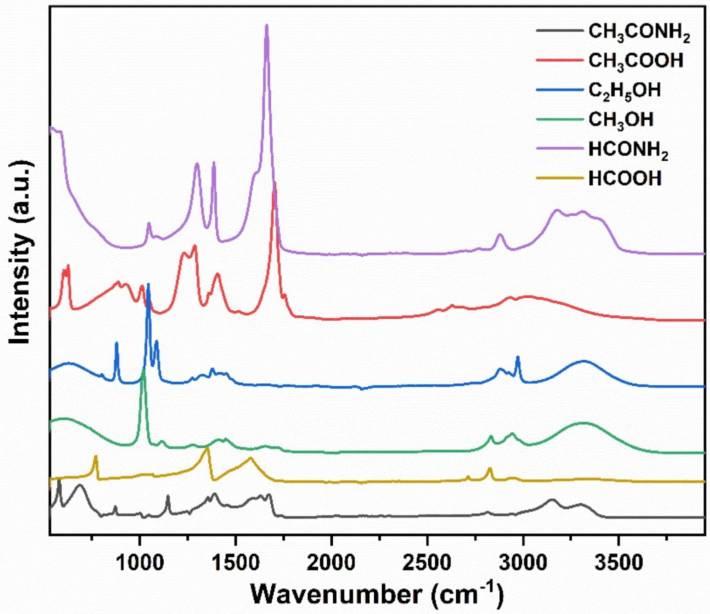

Figure S11: IR spectra of several products detected in $NH_3 + CO_2$ electrolysis

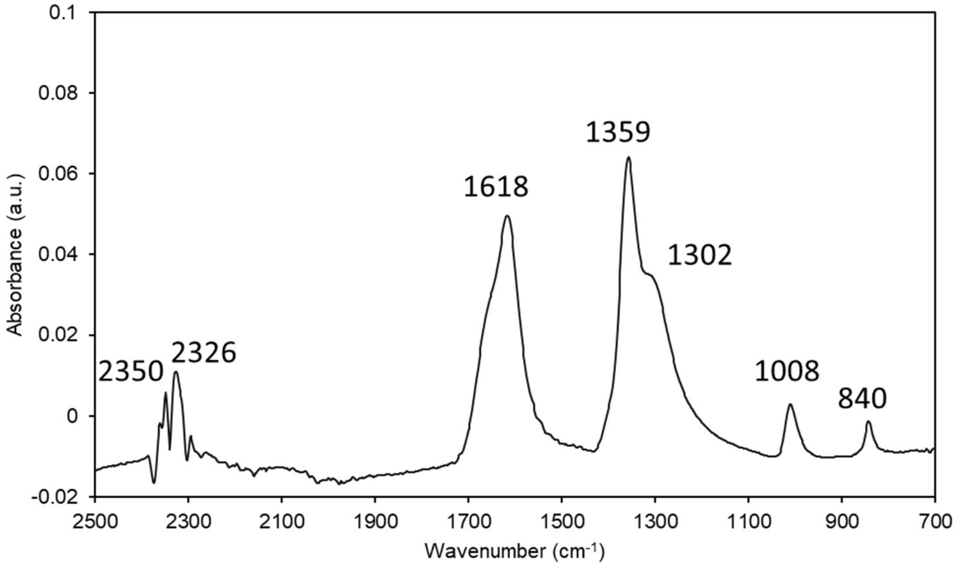

Figure S12: IR spectrum of the spectroelectrochemical setup with a CO_2 flow in 1M KOH, using an Ar flow in 1M KOH as the background. Peaks attributable to CO_2 and carbonate are present.

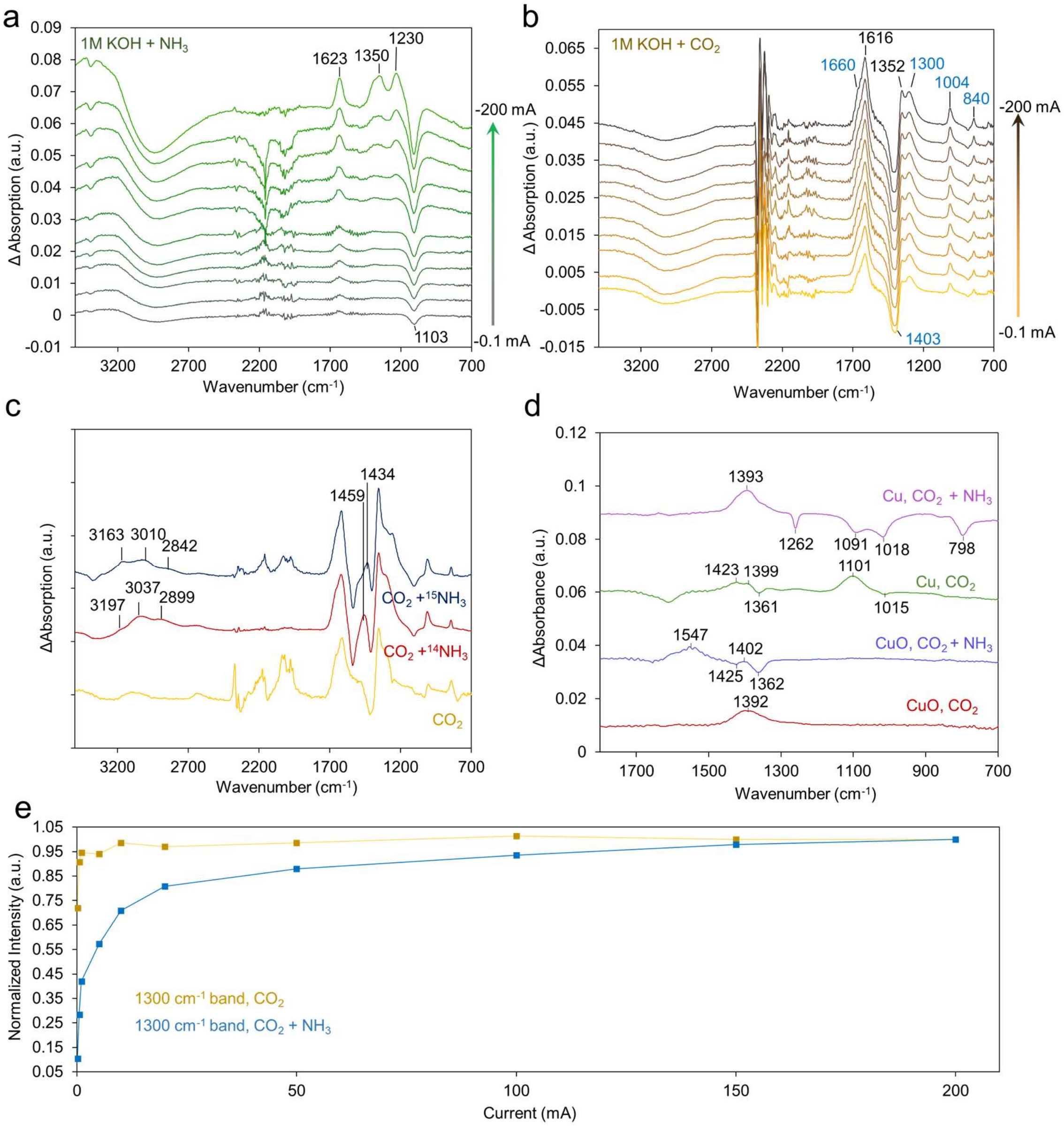

Figure S13: With the system as open circuit used as the background, spectra were acquired at select operating currents in the presence of NH_3 only (a) and CO_2 only (b). With CO_2 and $^{15}NH_3$ reactants, the spectra in (c) are used to identify the peaks belonging to $^{15}NH_4^+$ as it forms during reaction conditions. Subtracting out the (bi)carbonate contributions helps see weaker bands from intermediates (d). The rise of the bicarbonate peak, normalized to itself at 200 mA, is relatively slower with NH_3 present, indicating a slower generation of this species.

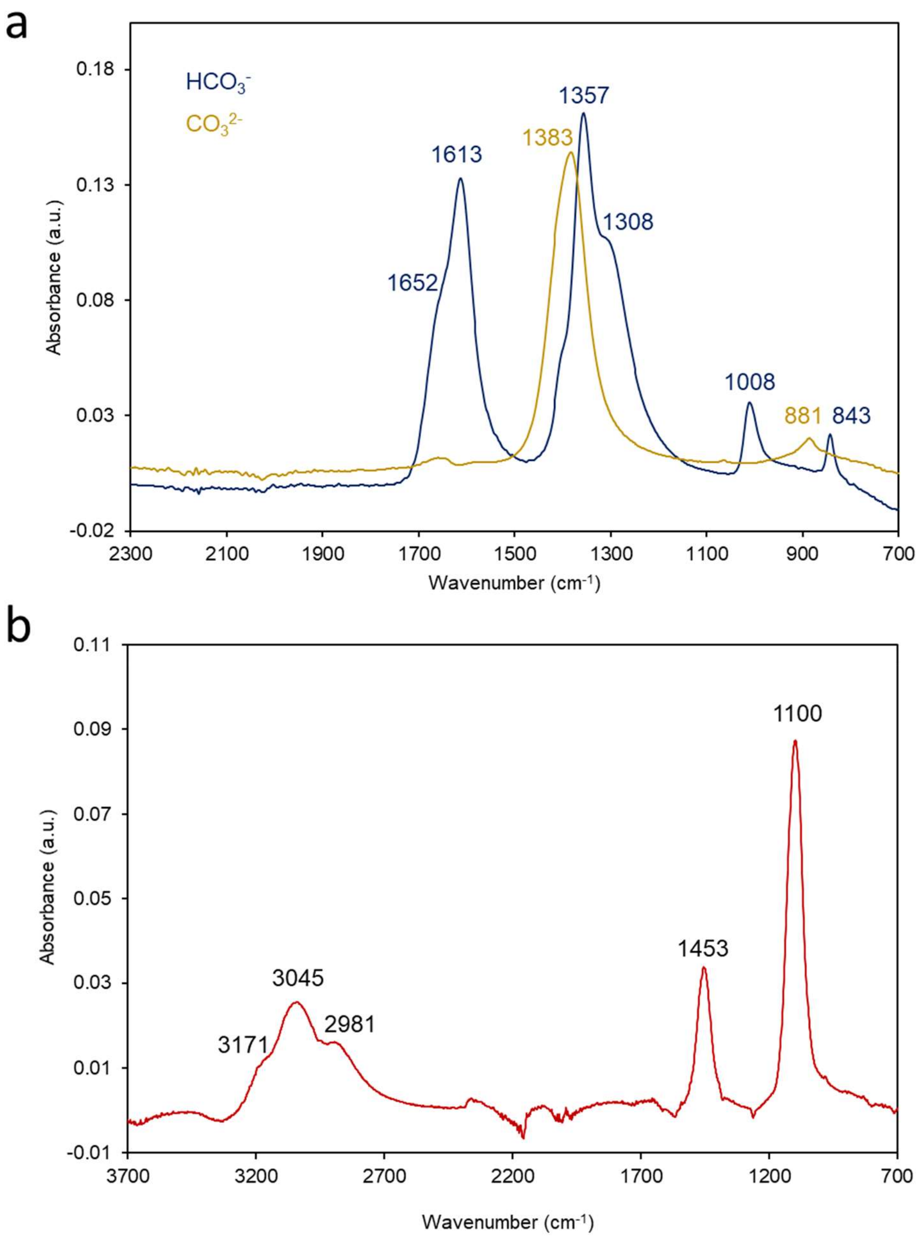

Figure S14: IR spectra of $KHCO_3$ and K_2CO_3 dissolved in water (a) and NH_4^+ (b)

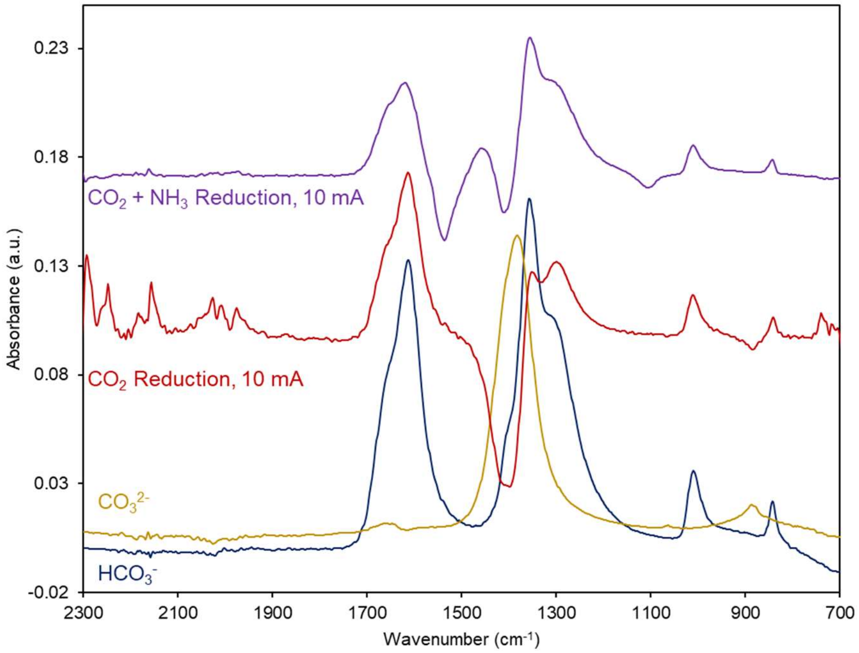

Figure S15: Overlaid spectra of (bi)carbonate and CO_2 reduction

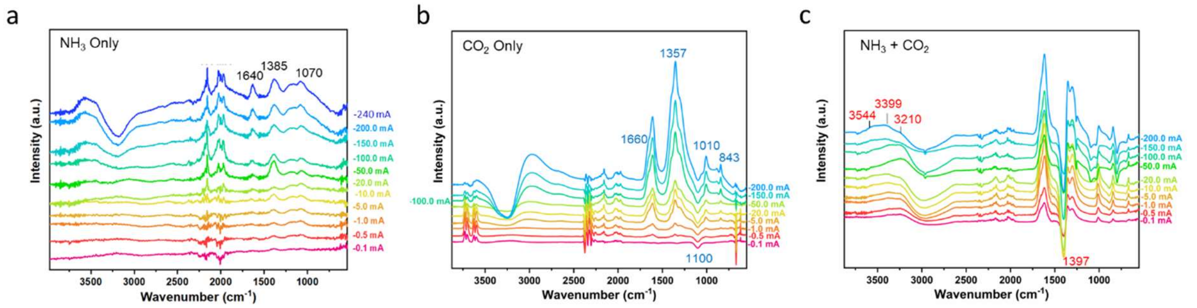

Figure S16: IR spectra of Cu catalysts, with NH_3 only (a), CO_2 only (b), and NH_3 + CO_2 (c).

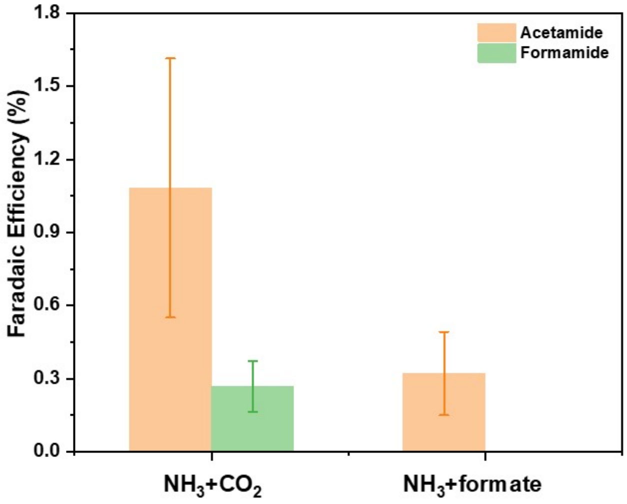

Figure S17: C-N bond formation using 150 mM NaCOOH as the C-source instead of CO_2 in otherwise identical conditions (1M KOH, -0.98V vs. RHE, Cu catalyst). The average partial current for acetamide in the formate case was 0.2 mA/cm^2.

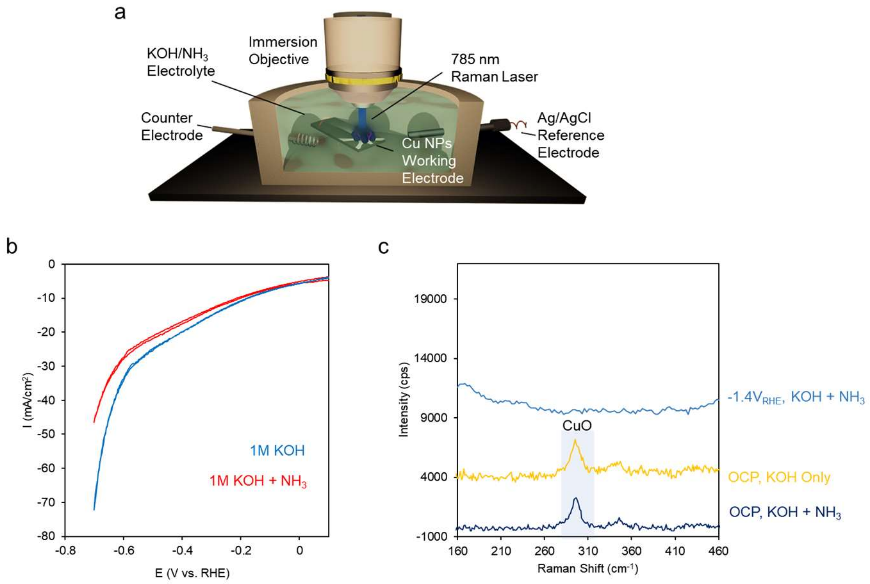

Figure S18: The addition of NH_3 to the electrolyte suppressed the water reduction current of Cu nanoparticles (a). Surface-enhanced Raman revealed the reduction of the surface oxide under a negative bias of -1.4V vs. RHE but no new bands that could be assigned to Cu-N species (a). Therefore, we believe that the NH_3 is near the electrode surface and alters the catalysis of the Cu without directly binding to it. Further, the decrease of current indicates that likely the NH_3 does not act as a proton donor for hydrogen evolution at rates higher than that of water.

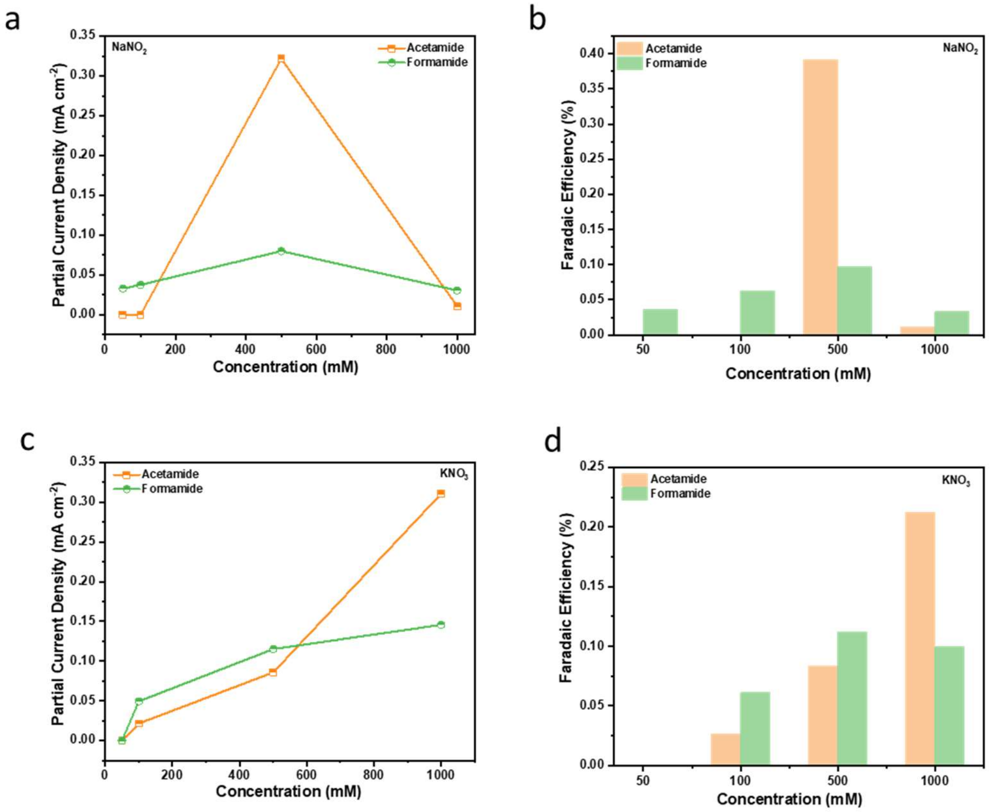

Figure S19: Partial current density (a) and Faradaic efficiency (b) for C-N products from $NaNO_2$ with Cu catalysts at -0.98V vs. RHE) as a function of reactant concentration in the liquid phase. Similarly, we measured the partial current density (a) and Faradaic efficiency (b) for C-N products from KNO_3 with Cu catalysts at -0.98V vs. RHE).

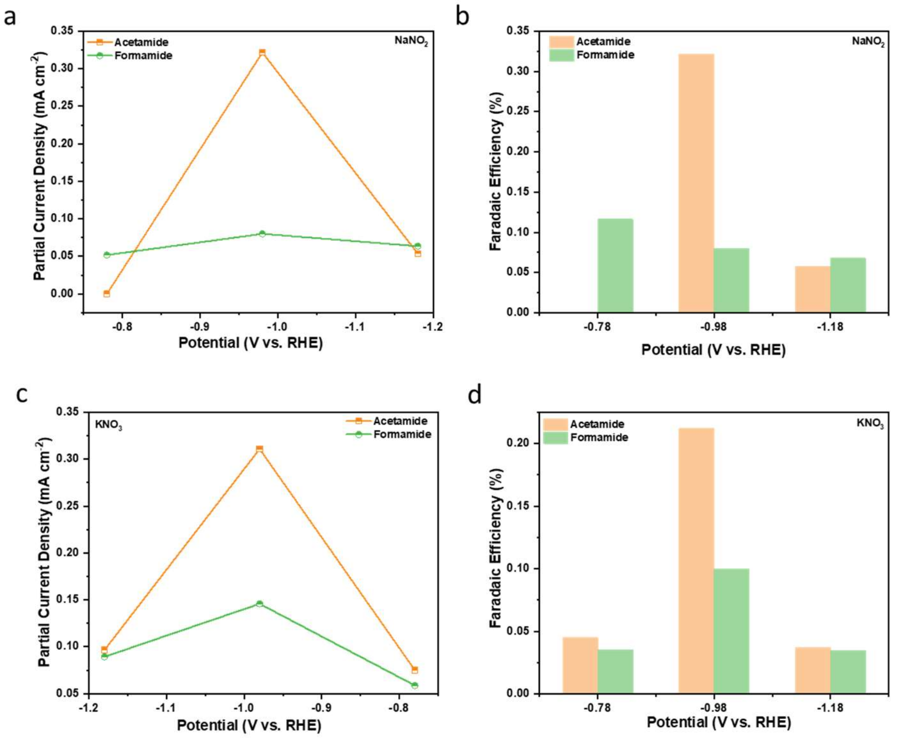

Figure S20: Partial current density (a) and Faradaic efficiency (b) for C-N products from NaNO$_2$ with Cu catalysts at -0.98V vs. RHE) as a function of potential. Further, we measured the partial current density (a) and Faradaic efficiency (b) for C-N products from KNO$_3$ with Cu catalysts at the above optimized concentration.

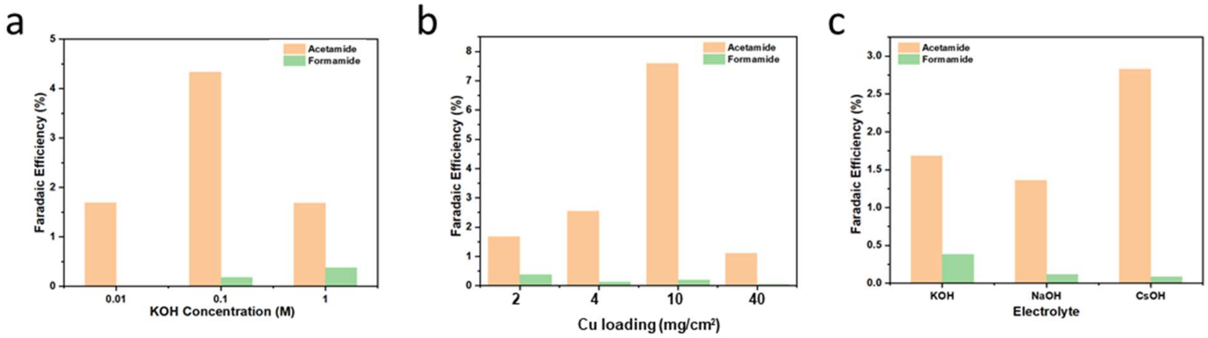

Figure S21: Optimization of reaction conditions with (a) different concentrations of KOH; (b) different amount of Cu nanoparticles; (c) electrolyte (1M) with different cations. The applied potential was -0.98V vs. RHE for this round of experiments.

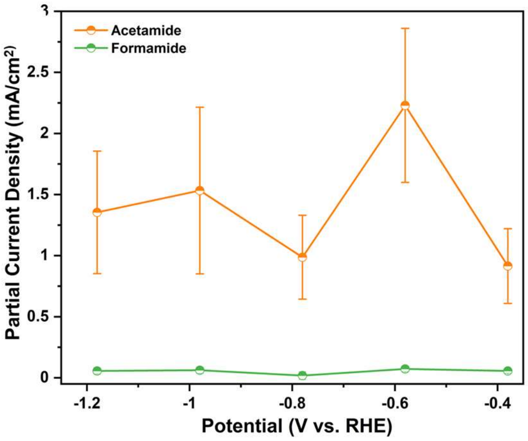

Figure S22: Partial current density for acetamide and formamide corresponding to the Faradaic efficiency at each potential in figure 6 in the main text.

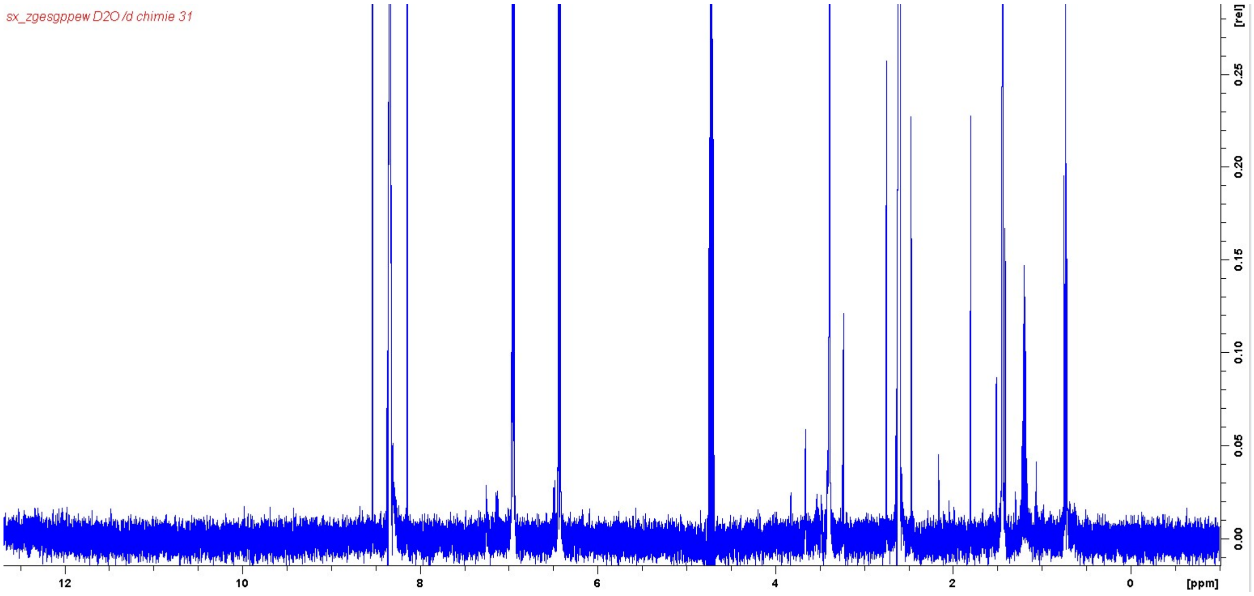

Figure S23: NMR spectrum under open circuit potential. 50 mM formate was added to 0.3 M NH_3 + 1M KOH for 1 hour and the solution probed afterwards. No formamide or acetamide could be detected.

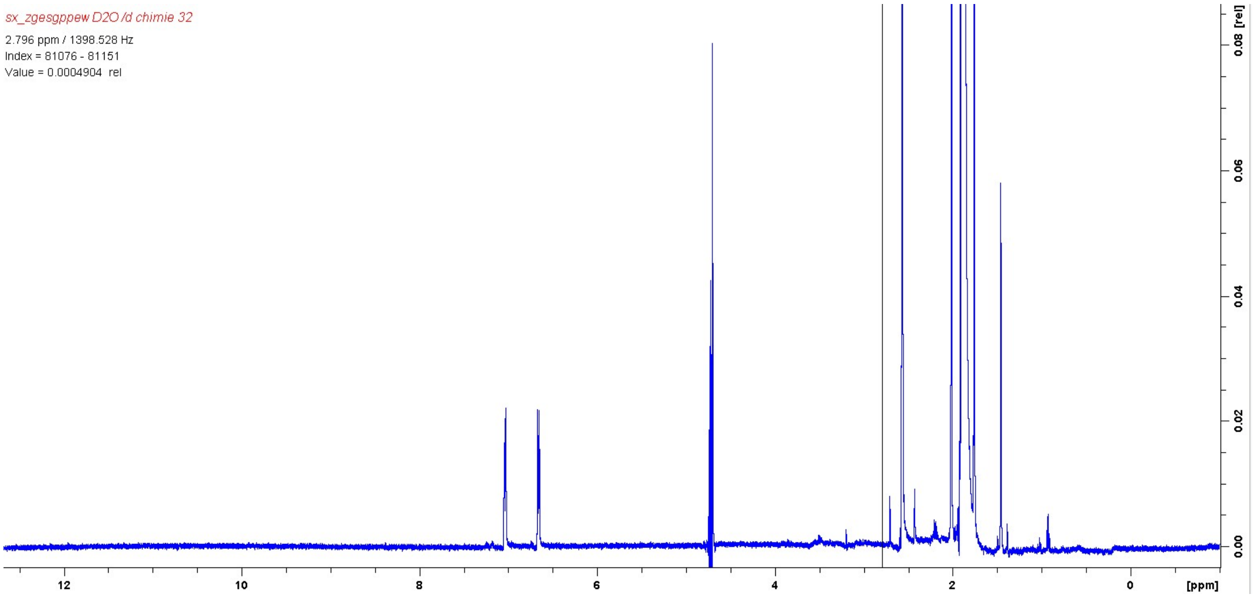

Figure S24: NMR spectrum under open circuit potential. 50 mM acetate was added to 0.3 M NH_3 + 1M KOH for 1 hour and the solution probed afterwards. No formamide or acetamide could be detected.

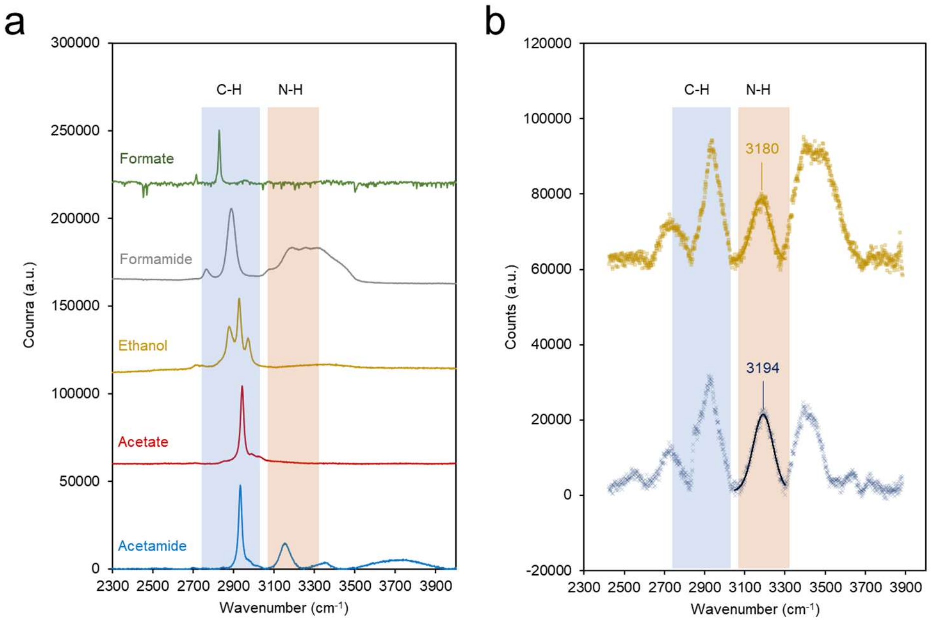

Figure S25: Raman spectra of several standards (a). C-H stretches are situated around 2900 cm^{-1} and N-H stretches are located around 3100-3200 cm^{-1}. Post electrolysis solutions were drop cast on a roughened Ag foil as a surface enhanced Raman substrate and their spectra taken with a 514 nm laser. Electrolysis with ^{14}N revealed a 3194 cm^{-1} band (b) matching that of acetamide. The N-H band of the solution using ^{15}N was situated at a lower frequency, 3180 cm^{-1} (c), as expected from the isotope shift.

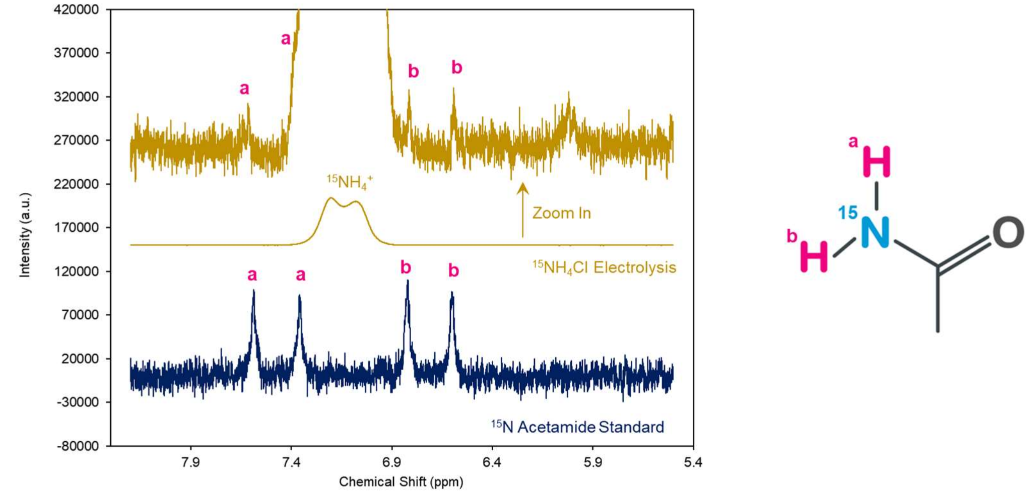

Figure S26: HNMR spectra of isotopically labeled acetamide and the NMR spectra of the acidified solution after CO_2 and $^{15}NH_4Cl$ electrolysis. Note: the spectra were acidified to pH 3 to render the peaks corresponding to the amine more apparent.

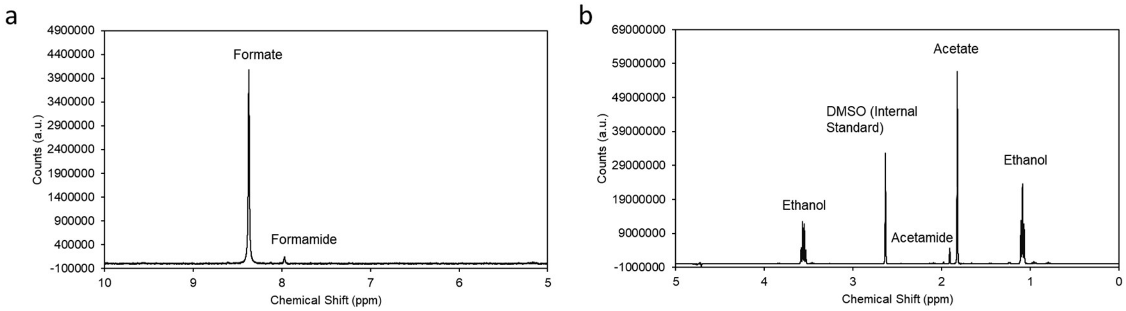

Figure S27: A typical spectrum after $CO_2 + NH_3$ electrolysis. The spectrum is broken up into two ranges (a, b) as they are zoomed into differently.